Physics of Fluids

RESEARCH ARTICLE | JANUARY 25 2024

Estimating viscoelastic, soft material properties using a modified Rayleigh cavitation bubble collapse time

Jin Yang (杨锦) ; Alexander McGhee ; Griffin Radtke ; Mauro Rodriguez, Jr. ; Christian Franck

Physics of Fluids 36, 017136 (2024)
https://doi.org/10.1063/5.0179368

Physics of Fluids ARTICLE pubs.aip.org/aip/pof

Estimating viscoelastic, soft material properties using a modified Rayleigh cavitation bubble collapse time

Cite as: Phys. Fluids **36**, 017136 (2024); doi: 10.1063/5.0179368
Submitted: 1 October 2023 · Accepted: 26 December 2023 ·
Published Online: 25 January 2024

Jin Yang (杨锦),[1,a)] Alexander McGhee,[2] Griffin Radtke,[2] Mauro Rodriguez, Jr.,[3] and Christian Franck[2]

AFFILIATIONS

[1]Department of Aerospace Engineering & Engineering Mechanics, The University of Texas at Austin, Austin, Texas 78712, USA
[2]Department of Mechanical Engineering, University of Wisconsin-Madison, Madison, Wisconsin 53706, USA
[3]School of Engineering, Brown University, Providence, Rhode Island 02912, USA

[a)]Author to whom correspondence should be addressed: jin.yang@austin.utexas.edu

ABSTRACT

Accurate determination of high strain rate ($>10^3$ 1/s) constitutive properties of soft materials remains a formidable challenge. Albeit recent advancements among experimental techniques, in particular inertial microcavitation rheometry (IMR), the intrinsic requirement to visualize the bubble cavitation dynamics has limited its application to nominally transparent materials. Here, in an effort to address this challenge and to expand the experimental capability of IMR to optically opaque materials, we investigated whether one could use the acoustic signature of the time interval between the bubble's maximum radius and first collapse time point, characterized as the bubble collapse time, to infer the viscoelastic material properties without being able to image the bubble directly in the tissue. By introducing a modified Rayleigh collapse time for soft materials, which is strongly dependent on the stiffness of the material at hand, we show that, in principle, one can obtain an order of magnitude or better estimate of the viscoelastic material properties of the soft material under investigation. Using a newly developed energy-based theoretical framework, we show that for materials stiffer than 10 kPa the bubble collapse time during a single bubble cavitation event can provide quantitative and meaningful information about the constitutive properties of the material at hand. For very soft materials (i.e., shear modulus less than 10 kPa), our theory shows that unless the collapse time measurement has very high precision and low uncertainties, the material property estimates based on the bubble collapse time only will not be accurate and require visual resolution of the full cavitation kinematics.

I. INTRODUCTION

Recent advances in clinical and biomedical procedures involving laser and ultrasound-based modalities rely on accurate representations of the underlying material tissue properties to mitigate collateral and unwanted damage.[1–7] Similarly, emerging designs of personal protective equipment are beginning to model the human–material interface,[8,9] once again requiring accurate material models of the underlying tissue and material properties. In many of these cases, the type of material properties sought is the constitutive behavior at high strain-rates ($> 10^3$ 1/s), which until recently was challenging to acquire experimentally due to the complex and compliant nature of these materials.[10] Perhaps, one of the most promising, and minimally invasive experimental techniques that recently emerged to address this need is inertial microcavitation rheometry (IMR). IMR is an inertial cavitation-based technique, specifically designed for the determination of the nonlinear viscoelastic constitutive properties of soft materials at high to ultra-high strain rates ($> 10^3$ 1/s).[10–16]

While this approach works well in transparent hydrogels and translucent tissues,[10,12,14–16] this approach has proven challenging in denser and more opaque materials, such as most tissues, due to its inherent requirement to optically resolve at least the first growth and collapse of the cavitation bubble. To circumvent that need, we asked whether the unique acoustic signature,[17–22] derived from radially emanating shock waves during laser initiation and collapse of the cavitating bubble, could be leveraged to inform about the material properties at hand. Specifically, the detection of the characteristic collapse time of the bubble, also known as the Rayleigh collapse time, t_c^{Rayleigh}, can be achieved by deploying far-field transducers or hydrophones, thus

removing the need to see inside the material. The classical Rayleigh collapse time is defined as the time it takes for the bubble to collapse in a given liquid, which can be derived from the continuity equation and the integration of the energy equation[23] as

$$t_c^{\text{Rayleigh}} = 0.914\,68\,R_{\max}\sqrt{\rho/p_a}, \tag{1}$$

where ρ denotes the mass density of the surrounding liquid and p_a denotes the ambient pressure. The proportionality constant 0.914 68 is known as the Rayleigh factor.

While the Rayleigh model and Rayleigh collapse time have historically been used to express the collapse time of a bubble within liquids,[24] recent experimental investigations of inertial cavitation in soft solids (i.e., hydrogels and biological tissues) have pointed toward the possibility of a similar characteristic Rayleigh collapse time within solids.

To investigate this, we carried out a theoretical study utilizing recently published laser-induced inertial cavitation (LIC) experimental data.[12,14,16] We found that a bubble's collapse time depended not only on the induced bubble size, mass density of the surrounding medium, and ambient pressure, similar to cavitation in a fluid, but also on the intrinsic viscoelastic properties of the surrounding solid. By deriving an energy-based framework for predicting the Rayleigh collapse time in various soft hydrogels, we were able to successfully estimate the viscoelastic material properties of these materials. The advantage of our new experimental-analytical framework presented here is that it lends itself for the estimation of the high-strain rate, viscoelastic material properties in nominally opaque materials as long as the characteristic collapse time and the maximum bubble radius can be experimentally measured or inferred. In cases where only t_c can be measured, we outline an empirical approach for a variety of commonly used hydrogels to determine the maximum bubble radius.

II. INERTIAL CAVITATION IN A VISCOELASTIC SOFT MATERIAL

A. Theoretical analysis of energy and bubble dynamics

As shown in Fig. 1(c), here we consider an ideal model of an inertial bubble oscillation in an infinite surrounding material such that the velocity in the far-field is zero. For an ideal, non-condensible gas inside the bubble, its potential energy is

$$E_{\text{PE}} = \int_{V_b} (p_\infty - p_b)\,\mathrm{d}V, \tag{2}$$

where $V_b = 4\pi R^3/3$ is the bubble volume; p_b is bubble internal pressure; and p_∞ is the far-field hydrostatic pressure.

The surrounding material is assumed to be incompressible and spherically symmetric whose deformation mapping follows

$$r(r_0, t) = \left(r_0^3 + R^3(t) - R_0^3\right)^{1/3}, \tag{3}$$

where r and r_0 are the current and reference radial positions. $R(t)$ is the time-dependent bubble radius, and R_0 is the radius of bubble at equilibrium. The velocity field outside the bubble can be calculated as the time derivative of Eq. (3),

$$v = \frac{\dot{R}R^2}{r^2}, \tag{4}$$

which is also spherically symmetric.

The kinetic energy of the surrounding material is

$$E_{\text{KE}} = \int_{V_s} \frac{1}{2}\rho v^2 \mathrm{d}V = 2\pi\rho\dot{R}^2R^3, \tag{5}$$

where V_s is the volume of the surrounding material.

We assume that the temperature change in the surrounding material is small enough such that the change in internal energy can be neglected.

The stored surface energy at the bubble wall is

$$E_{\text{SFE}} = S_b\sigma = 4\pi R^2\sigma, \tag{6}$$

where S_b is the bubble surface area and equals $4\pi R^2$ for a spherical cavity. σ is the surface tension coefficient at the bubble wall.

By modeling the elastic contribution of the surrounding material as a neo-Hookean (NH) hyperelastic material, its stored elastic energy can be calculated as

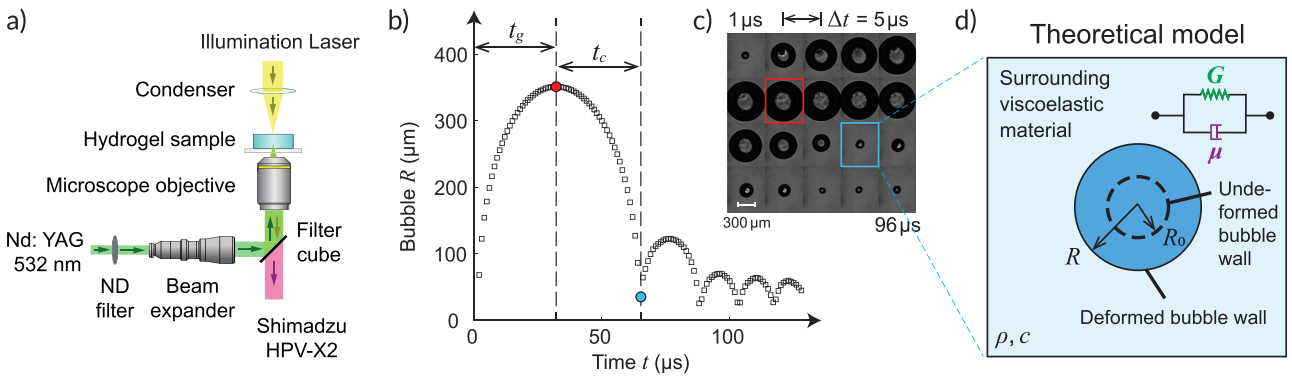

FIG. 1. (a) The experimental setup of a pulsed-laser-induced inertial cavitation (LIC) event created within a hydrogel sample. (b) A typical experimentally measured bubble R vs t curve for a LIC event in a soft 3% polyacrylamide hydrogel sample. The bubble growth time t_g is defined as the time between the bubble initiation and its maximum radius (red dot), and the bubble collapse time t_c is defined as the time between the maximum radius and the first collapse time point (blue dot). (c) Twenty selected frames in the LIC event in subfigure (b) were captured by the high-speed camera. (d) The illustrated model is for an inertial cavitation bubble occurring within a bulk soft material modeled as a neo-Hookean Kelvin–Voigt (NHKV) viscoelastic material.

$$E_{\text{Elastic}} = \int_{V_s} W_{\text{NH}}\, \mathrm{d}V. \tag{7}$$

W_{NH} is the neo-Hookean strain energy density,

$$W_{\text{NH}} = \frac{G}{2}\left[\left(\frac{r_0}{r}\right)^4 + 2\left(\frac{r}{r_0}\right)^2 - 3\right], \tag{8}$$

where G is the shear modulus of the surrounding material. For each material point whose reference position is r_0 and time-dependent position is $r(t)$, we introduce a stretch ratio parameter $\lambda := r/r_0$. Therefore, Eq. (7) can be further simplified as (detailed derivation steps are summarized in Appendix)

$$E_{\text{Elastic}} = 2\pi G\left(R^3 - R_0^3\right)\left(\frac{2}{3} - \frac{R_0}{R} + \frac{R^2}{R^2 + RR_0 + R_0^2}\right). \tag{9}$$

We also assume that the surrounding material has a Newtonian viscosity. The spatial velocity gradient tensor is defined as

$$\mathbf{L} = \nabla \mathbf{v} = \begin{bmatrix} -\frac{2R^2\dot{R}}{r^3} & 0 & 0 \\ 0 & \frac{R^2\dot{R}}{r^3} & 0 \\ 0 & 0 & \frac{R^2\dot{R}}{r^3} \end{bmatrix}. \tag{10}$$

The rate of deformation tensor $\mathbf{D}$ is the symmetric part of $\mathbf{L}$,

$$\mathbf{D} = \frac{1}{2}\left(\mathbf{L} + \mathbf{L}^{\top}\right). \tag{11}$$

The viscous dissipation can be calculated in the following form:

$$D_{\text{Visc}} = \int_{V_s} \mu \mathbf{D} : \mathbf{D}\, \mathrm{d}V = 8\pi\mu R\dot{R}^2, \tag{12}$$

where μ is the Newtonian viscosity coefficient.

The Lagrangian for the inertial cavitation system can be further defined as

$$\mathscr{L} = E_{\text{KE}} - E_{\text{PE}} - E_{\text{SFE}} - E_{\text{Elastic}}. \tag{13}$$

Following the principle of least action, we derive the Euler–Lagrange equation as[25–27]

$$\frac{\mathrm{d}}{\mathrm{d}t}\left(\frac{\partial \mathscr{L}}{\partial \dot{R}}\right) - \frac{\partial \mathscr{L}}{\partial R} + \frac{\partial D_{\text{Visc}}}{\partial \dot{R}} = 0. \tag{14}$$

Using Eqs. (2)–(12) in Eq. (14), we recover the modified Rayleigh–Plesset equation to describe inertial cavitation bubble dynamics in an infinite, Kelvin–Voigt-type viscoelastic soft material where the surrounding material is modeled as a hyperelastic neo-Hookean branch in parallel with a linear (Newtonian) viscous dashpot [see Fig. 1(d)],[10]

$$\ddot{R}R + \frac{3}{2}\dot{R}^2 = \frac{1}{\rho}\left(p_b - \frac{2\sigma}{R} - p_\infty + S_{\text{int}}\right), \tag{15}$$

where S_{int} is the stress integral of the following form:

$$S_{\text{int}} = -\frac{G}{2}\left[5 - \left(\frac{R_0}{R}\right)^4 - \frac{4R_0}{R}\right] - \frac{4\mu\dot{R}}{R}. \tag{16}$$

If accounting for compressibility effects in the surrounding material is desired, a modified Keller–Miksis equation [see Eq. (17)] can be applied to account for first order compressibility effects. The modified Keller–Miksis equation (17) will reduce to the modified Rayleigh–Plesset equation (15) at the limit $c \to \infty$,

$$\begin{aligned}\left(1 - \frac{\dot{R}}{c}\right)R\ddot{R} + \frac{3}{2}\left(1 - \frac{\dot{R}}{3c}\right)\dot{R}^2 &= \frac{1}{\rho}\left(1 + \frac{\dot{R}}{c}\right)\left(p_{\text{b}} - p_\infty - \frac{2\gamma}{R} + S_{\text{int}}\right) \\ &\quad + \frac{1}{\rho}\frac{R}{c}\overline{\left(p_{\text{b}} - \frac{2\gamma}{R} + S_{\text{int}}\right)}.\end{aligned} \tag{17}$$

Following Estrada *et al.*,[10] the bubble's internal gas composition is modeled as a mixture gas of water vapor and non-condensible, ideal gas, whose pressure is

$$p_b = p_{g0}\left(\frac{R_0}{R}\right)^{3k} + p_{\text{v,sat}}(T_b), \tag{18}$$

where k equals the specific heat capacity ratio if we assume the bubble internal gas to be adiabatic. Then, T_b is the effective averaged bubble internal temperature. $p_{\text{v,sat}}(T_b)$ is the saturation pressure of water vapor at temperature T_b. p_{g0} is the partial pressure of the non-condensible gas at equilibrium satisfying

$$p_{g0} = p_\infty - p_{\text{v,sat}}(T_\infty) + \frac{2\sigma}{R_0}. \tag{19}$$

Equations (15)–(19) are implemented using a fifth-order explicit Dormand–Prince Runge–Kutta method with adaptive step-size control to evolve the governing equations forward in time.[28,29]

B. Theoretical analysis of the collapse time in an infinite viscoelastic material

To develop an analytical expression for the bubble collapse time, t_c, we use an energy-based approach making the following assumptions.[30] We constrain ourselves to the time period up to the first bubble collapse, where we describe the dynamics of the cavitation bubble to be inertially and elastically dominated.[10,12,14] Thus, we disregard the effects of viscosity, the bubble's internal gas contents, and temperature changes in the surrounding material, and we also assume that the total energy is conserved before the first violent collapse. Non-negligible acoustic radiation energy transfer and viscous dissipation occur primarily after the first bubble collapse, and in particular, for violent collapses [i.e., Mach number > 0.1 (Refs. 12 and 29)]. Given our assumptions, the total energy, $\mathscr{E}$, is then defined as

$$\begin{aligned}\mathscr{E} &= E_{\text{KE}} + E_{\text{PE}} + E_{\text{SFE}} + E_{\text{Elastic}} \\ &= 2\pi\rho\dot{R}^2R^3 + \frac{4}{3}\pi R^3(p_\infty - p_b) + 4\pi R^2\sigma \\ &\quad + 2\pi G\left(R^3 - R_0^3\right)\left(\frac{2}{3} - \frac{R_0}{R} + \frac{R^2}{R^2 + RR_0 + R_0^2}\right),\end{aligned} \tag{20}$$

where the contributions of the bubble's internal pressure p_b and viscous dissipation are further neglected due to our above-mentioned model assumption. When the bubble reaches its maximum radius, i.e., $R = R_{\max}$, $\dot{R} = 0$, we also have

$$\mathscr{E} = \frac{4}{3}\pi R_{\max}^3 p_\infty + 4\pi R_{\max}^2 \sigma + 2\pi G\left(R_{\max}^3 - R_0^3\right)\left(\frac{2}{3} - \frac{R_0}{R_{\max}} + \frac{R_{\max}^2}{R_{\max}^2 + R_{\max}R_0 + R_0^2}\right). \tag{21}$$

Combining Eqs. (20) and (21), we can solve an explicit form for $\dot{R}$,

$$\dot{R}^2 = \frac{2}{3}\frac{p_\infty}{\rho}\left(\frac{R_{\max}^3}{R^3} - 1\right) + \frac{2\sigma}{\rho R}\left(\frac{R_{\max}^2}{R^2} - 1\right) + \frac{G}{\rho}\left(\frac{R_{\max}^3}{R^3} - \frac{R_0^3}{R^3}\right)\left(\frac{2}{3} - \frac{R_0}{R_{\max}} + \frac{R_{\max}^2}{R_{\max}^2 + R_{\max}R_0 + R_0^2}\right) - \frac{G}{\rho}\left(1 - \frac{R_0^3}{R^3}\right)\left(\frac{2}{3} - \frac{R_0}{R} + \frac{R^2}{R^2 + RR_0 + R_0^2}\right). \tag{22}$$

Equation (22) can be rearranged for a differential equation for R,

$$\left|\frac{\mathrm{d}R}{\mathrm{d}t}\right| = \left[\frac{2}{3}\frac{p_\infty}{\rho}\left(\frac{R_{\max}^3}{R^3} - 1\right) + \frac{2\sigma}{\rho R}\left(\frac{R_{\max}^2}{R^2} - 1\right) + \frac{G}{\rho}\left(\frac{R_{\max}^3}{R^3} - \frac{R_0^3}{R^3}\right)\left(\frac{2}{3} - \frac{R_0}{R_{\max}} + \frac{R_{\max}^2}{R_{\max}^2 + R_{\max}R_0 + R_0^2}\right) - \frac{G}{\rho}\left(1 - \frac{R_0^3}{R^3}\right)\left(\frac{2}{3} - \frac{R_0}{R} + \frac{R^2}{R^2 + RR_0 + R_0^2}\right)\right]^{1/2}. \tag{23}$$

If $R_0/R_{\max} \ll 1$, we can further integrate (23) from $t : t_{\max} \to t_c$ on the left-hand side where $t_{\max}$ and t_c correspond to the time at maximum bubble radius and the time at first bubble collapse, respectively, i.e., $R : R_{\max} \to R_0 \approx 0$ on the right-hand side to obtain the approximated collapse time t_c. Furthermore, the left-hand side of Eq. (23) can be simplified as $-\mathrm{d}R/\mathrm{d}t$ since the radial velocity of the bubble surface is negative as the bubble is collapsing,

$$t_c = \left(\frac{2}{3} + \frac{5}{3}\frac{G}{p_\infty}\right)^{-\frac{1}{2}}\left[\int_0^1 \frac{\xi^{3/2}}{\sqrt{1-\xi^3}}\,\mathrm{d}\xi\right] R_{\max}\sqrt{\frac{\rho}{p_\infty}}, = \left(\frac{2}{3} + \frac{5}{3}\frac{G}{p_\infty}\right)^{-\frac{1}{2}} 0.747\, R_{\max}\sqrt{\frac{\rho}{p_\infty}}. \tag{24}$$

One particular limit case is when the surrounding material is water, i.e., $G \to 0$, (24) will recover the classic Rayleigh collapse time as shown in Eq. (1).[23]

Finally, to facilitate comparison and analysis for each type of material, we introduce the non-dimensionalized collapse time, ψ, as

$$\psi = t_c R_{\max}^{-1}(\rho/p_\infty)^{-1/2}. \tag{25}$$

III. RESULTS

In this section, we estimate the viscoelastic properties of three commonly used hydrogels using our newly derived modified Rayleigh collapse time approach based on (i) the knowledge of t_c and $R_{\max}$ or (ii) solely the measurement of the bubble collapse time, t_c. The general work flow of estimating the material properties is given by Algorithm 1. In all instances, the overall goal is to define a loss function that minimizes the least squares difference between the estimated and experimentally measured (or informed) non-dimensional collapse time, ψ.

Since the modified Rayleigh collapse time (24) requires knowledge of $R_{\max}$, its value must be supplied in order to calculate $\psi_{\exp}$. If $R_{\max}$ is not known, it can be deduced either from the data shown in Fig. 2 relating t_c with $R_{\max}$ for the hydrogels presented here, found elsewhere in the literature or compiled by the user themselves. For semi-opaque or thinner cross section opaque samples, cavitation generation is still possible via laser nucleation, where $R_{\max}$ and t_c can be experimentally measured to establish their relationship, as shown in Fig. 2. For fully opaque tissues, recent developments using ultrasound focusing can induce inertial cavitation events and measure t_c.[22,32] It is also possible to measure $R_{\max}$ values for fully opaque samples using high-speed x-ray phase-contrast imaging.[33] However, it still remains extremely challenging to directly measure $R_{\max}$ for opaque samples. If the bubble equilibrium radius R_0 can be measured after pulsed inertial cavitation using optical coherence tomography (OCT)[34,35] or magnetic resonance imaging (MRI),[36] we can write $R_{\max}$ as a function of the surrounding material's shear modulus G using the maximum circumferential stretch ratio, as shown in supplementary material Eqs. (S1) and (S2), and extract surrounding material's properties using Algorithm 1.

In our case and for the materials presented here (Fig. 2), we quantitatively measured the bubble collapse time for each laser-induced inertial cavitation (LIC) event by analyzing the fitted R vs t curve. The experimental measurements obtained from LIC events in polyacrylamide (PAAM),[12] agarose,[14] and gelatin[16] hydrogels are shown in Fig. 2 and summarized in Table I.

ALGORITHM 1: Extracting unknown material viscoelastic properties using the bubble's collapse time.

Data: t_c, $R_{\max}$ (if known), initially guessed shear modulus G_i
Result: Viscoelastic material properties: G, μ
if $R_{\max}$ *is unknown* **then**
  Estimate $R_{\max}$ from Fig. 2;
  Or measure equilibrium radius R_0 and write $R_{\max}$ as a function of shear modulus G using the maximum circumferential stretch ratio as shown in Eqs. (S1) and (S2)
end
Calculate $\psi_{\exp} = t_c R_{\max}^{-1}(\rho/p_\infty)^{-1/2}$;
Initialize $Loss > \varepsilon$, $G = G_i$;
while $Loss > \varepsilon$ **do**
  Calculate ψ using (26);
  Update $Loss = |\psi - \psi_{\exp}|^2$;
  Update G using pattern search optimization scheme;
end
Calculate estimated viscosity μ using (31) or (32);

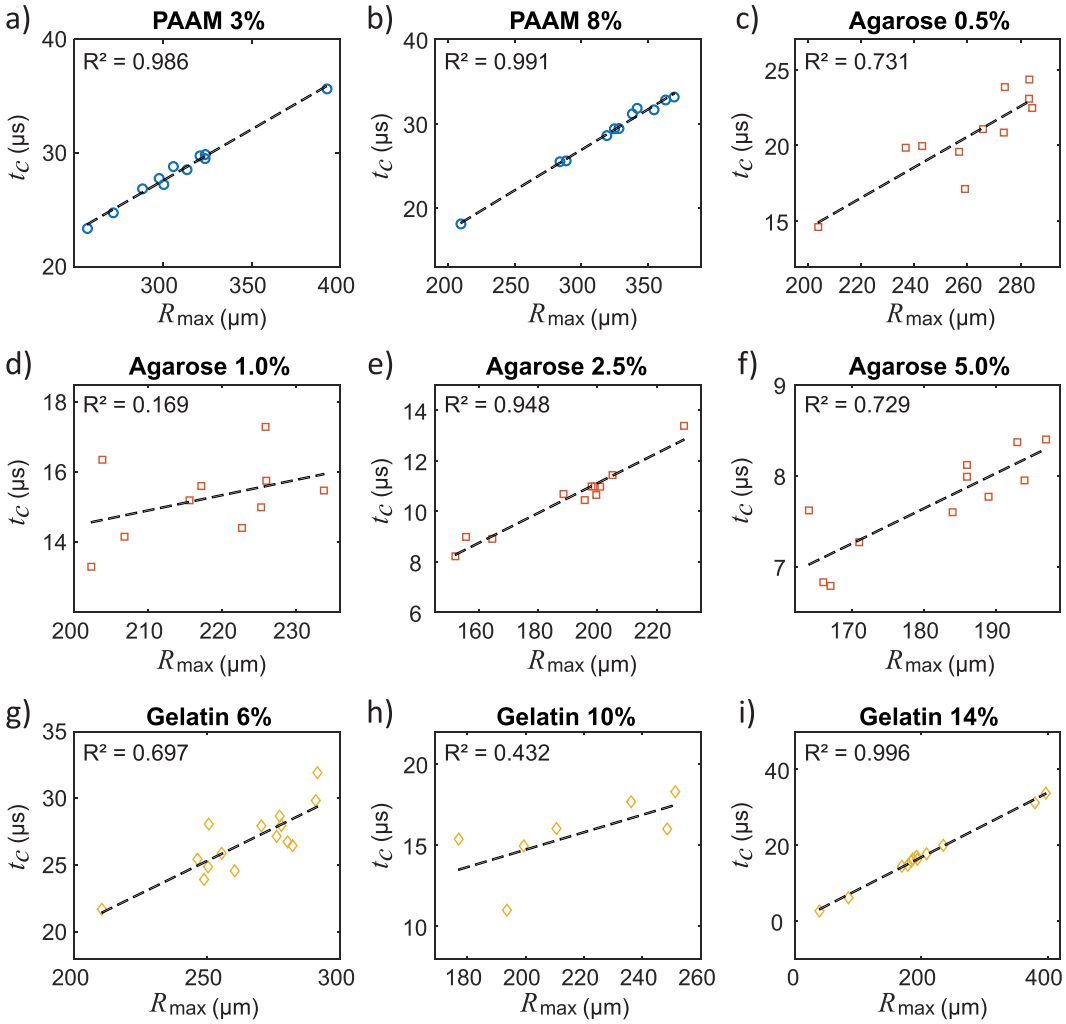

FIG. 2. Summary of experimentally measured laser-induced inertial cavitation (LIC) collapse times in various bulk soft materials: (a) and (b) 3% and 8% polyacrylamide (PAAM); (c)–(f) 0.5%, 1.0%, 2.5%, and 5.0% agarose hydrogels; and (g)–(i) 6%, 10%, and 14% gelatin hydrogels.

TABLE I. Summary of the utilized viscoelastic material properties and their maximum and equilibrium bubble radius and maximum circumferential stretch ratios (λ_{max}) in LIC experiments in Sec. III.[12,14,16] All these material properties are also summarized and discussed in Bremer-Sai *et al.*[31]

Material	G (kPa)	μ (Pa · s)	R_{max} (μm)	λ_{max}
PAAM 3%	8.31 ± 0.43	0.093 ± 0.073	301.72 ± 26.87	10.3 ± 0.91
PAAM 8%	15.09 ± 4.35	0.209 ± 0.180	330.26 ± 30.36	7.1 ± 0.65
Agarose 0.5%	27.82 ± 8.56	0.17 ± 0.09	260.36 ± 24.88	7.54 ± 0.30
Agarose 1.0%	58.12 ± 9.38	0.30 ± 0.09	218.57 ± 10.44	6.57 ± 0.17
Agarose 2.5%	114.64 ± 4.85	0.11 ± 0.05	185.55 ± 19.45	4.32 ± 0.08
Agarose 5.0%	282.37 ± 22.83	0.50 ± 0.07	184.41 ± 11.84	3.01 ± 0.15
Gelatin 6%	12.78 ± 3.69	0.027 ± 0.022	184.0 ± 18.2	3.29 ± 0.36
Gelatin 10%	29.85 ± 6.20	0.055 ± 0.061	175.9 ± 21.1	2.99 ± 0.36
Gelatin 14%	101.50 ± 4.01	0.166 ± 0.208	171.0 ± 28.2	2.60 ± 0.19

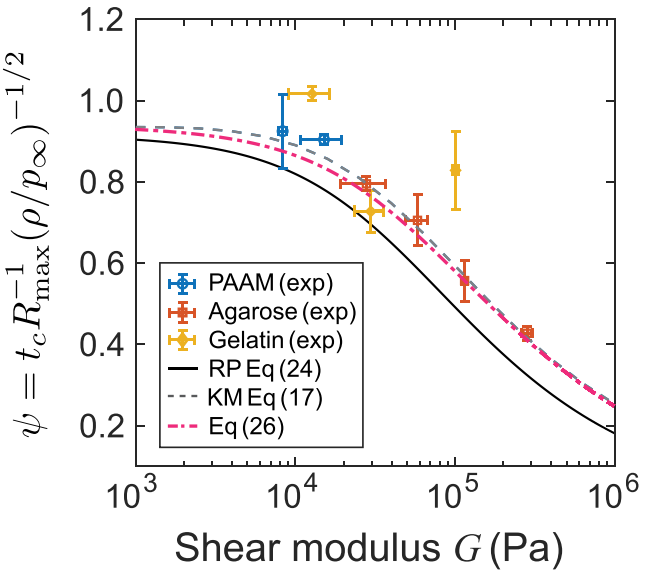

FIG. 3. Comparison of numerically simulated and experimentally measured bubble collapse times in bulk gel systems.

To facilitate comparison and analysis across all types of material, we non-dimensionalize all experimentally measured collapse time data points from Fig. 2 by using the non-dimensional parameter ψ (25). The non-dimensionalized data points are plotted in Fig. 3, where the black line represents (24) and serves as a reference for comparison. Additionally, we performed direct numerical simulations for Eq. (17) with different values of $R_{\max}$, which are depicted as dashed lines with corresponding values of $R_{\max}$.

The overall shape and trend of our predictions agree well with the experimental observations, demonstrating that the collapse time of cavitation bubbles is influenced not only by their size ($R_{\max}$), the mass density, and ambient pressure of the surrounding material, but also by the mechanical properties of the material itself. Specifically, we predict, consistent with experimental measurements, that a stiffer surrounding material with a higher shear modulus (G) results in a shorter collapse time as long as the shear modulus is sufficiently large (> 10 kPa). As the shear modulus drops below 10 kPa, the collapse time approaches the classical Rayleigh collapse time asymptotically and becomes nearly independent of the material's shear modulus. When the ratio $G/p_\infty \ll 1$, as indicated by Eq. (24) and Fig. 3, the collapse time in a gel material follows the classic Rayleigh collapse time expressed in Eq. (1).

However, as can be clearly seen from Fig. 3, our expression for the modified Rayleigh collapse time in Eq. (24) consistently underestimates the experimental measurements. This discrepancy arises due to additional factors such as material viscosity, internal gas dynamics within the bubble, and the radiation of acoustic waves, all which slow down the bubble dynamics, and lead to a prolonged first collapse time. In comparison, direct numerical simulations accurately predict the first collapse time for various hydrogel types, except for the gelatin 10% and 14% hydrogels. To address this deviation from our prediction, we introduce a new modified Rayleigh collapse time, $t_c^{\text{corrected}}$, with an empirically derived correction factor θ accounting for some of the above-mentioned effects. Its non-dimensional version, $\psi^{\text{corrected}}$, can be seen in Fig. 3 dot-dash curve and forms the basis for estimating the material properties shown in Table II using Algorithm 1,

$$t_c^{\text{corrected}} = \theta(R_{\max}, \mu)\left(\frac{2}{3} + \frac{5}{3}\frac{G}{p_\infty}\right)^{-\frac{1}{2}} 0.747\, R_{\max}\sqrt{\frac{\rho}{p_\infty}}, \tag{26}$$

where non-dimensional parameters θ_1 and θ_2 are for static, i.e., low polymer chain bond mobility, and dynamic, i.e., high polymer chain bond mobility, crosslinks hydrogels, respectively,

$$\theta_1 = a_1 + b_1\left[\tanh c_1\left(\log_{10}\mu - d_1\right)\right], \tag{27}$$

$$\theta_2 = a_2 + b_2\left[\tanh c_2\left(\log_{10}\mu - d_2\right)\right], \tag{28}$$

where μ is in the unit of Pa · s; $\{a_1, b_1, c_1\} = \{1.362, 0.335, 2\}$ and $\{a_2, b_2, c_2\} = \{1.589, 0.562, 1.75\}$ are two sets of constants for static and dynamic crosslinks gels, respectively. Variables d_1 and d_2 are functions of maximum bubble radius, which are fitted using quadratic equations as

$$d_1 = -1.13\left(\log_{10}R_{\max}\right)^2 - 7.572\log_{10}R_{\max} - 12.83, \tag{29}$$

TABLE II. Estimated viscoelastic material properties using only collapse time t_c and the maximum bubble radius ($R_{\max}$) in LIC experiments.

		Fitted material properties using $\{t_c, R_{\max}\}$		Fitted material properties using $\{t_c\}$ only	
Material	$\psi = t_c R_{\max^{-1}}(\rho/p_\infty)^{-1/2}$	G (kPa)	μ (Pa · s)	G (kPa)	μ (Pa · s)
PAAM 3%	0.925 ± 0.013	1.62 ± 1.17	0.0233 ± 0.0156	1.46 ± 0.21	0.0230 ± 0.0027
PAAM 8%	0.904 ± 0.017	3.98 ± 2.30	0.0468 ± 0.0205	3.92 ± 1.66	0.0479 ± 0.0124
Agarose 0.5%	0.795 ± 0.063	22.72 ± 14.09	0.131 ± 0.0395	21.70 ± 6.62	0.1336 ± 0.0187
Agarose 1.0%	0.705 ± 0.051	45.97 ± 14.08	0.189 ± 0.0289	44.26 ± 7.51	0.1880 ± 0.0145
Agarose 2.5%	0.557 ± 0.017	120.88 ± 15.30	0.282 ± 0.0133	120.54 ± 11.93	0.2818 ± 0.0100
Agarose 5.0%	0.427 ± 0.017	270.04 ± 28.75	0.372 ± 0.0129	268.59 ± 6.060	0.3714 ± 0.0027
Gelatin 6%	1.018 ± 0.052	0.101 ± 0.0014	$0.0026 \pm 2.34 \times 10^{-5}$	0.100 ± 0	0.0026 ± 0
Gelatin 10%	0.729 ± 0.096	58.82 ± 37.25	0.0992 ± 0.0202	52.105 ± 12.785	0.0989 ± 0.0098
Gelatin 14%	0.830 ± 0.064	22.46 ± 16.48	0.0681 ± 0.0241	300.898 ± 46.570	0.1628 ± 0.0052

$$d_2 = -0.2641\left(\log_{10}R_{\max}\right)^2 - 1.74\log_{10}R_{\max} - 3.356, \quad (30)$$

where $R_{\max}$ is in the unit of m.

Finally, it should be noted that our predictions indicate that smaller bubbles exhibit higher values of ψ, and there is a non-monotonic trend in ψ vs G when the bubble size is smaller than 80 μm (see supplementary material Sec. S3). These deviations might be due to the increasing role of surface tension for smaller bubbles for cases when $R_{\max}$ is no longer significantly greater than R_0, which is an implicit assumption in the derivation of Eq. (24). As this warrants a deeper investigation beyond the purpose of our initial study here, we limit the applicability of our modified Rayleigh approach to larger bubbles with nominal radii above 80 μm.

A. Estimation of viscoelastic material properties using the modified Rayleigh collapse time

As described in Algorithm 1, the material shear modulus G is estimated via a least squares minimization procedure of the non-dimensional collapse time, ψ (steps 1–11), after which the material viscosity is calculated using the following two equations obtained by fitting the data presented in Fig. 4 for statically (i.e., PAAM and agarose) and dynamically (i.e., gelatin) crosslinked hydrogels, respectively (step 12),

$$\mu^{\text{Fit1}} = 20.70 \times 10^{-9.48/\log_{10}(G+156.96)}, \quad (31)$$

$$\mu^{\text{Fit2}} = 656.15 \times 10^{-18.09/\log_{10}(G+1287.81)}. \quad (32)$$

Material properties μ and G are in the units of Pa · s and Pa, respectively. Using the experimentally measured collapse time and $R_{\max}$ values shown in Table I, all estimated material properties using our new modified Rayleigh collapse time approach (i.e., Algorithm 1) are summarized in Table II for the case (i) when both t_c and $R_{\max}$ are known and (ii) if only t_c is available but $R_{\max}$ can be deduced from a prior database or correlation as presented in Fig. 2.

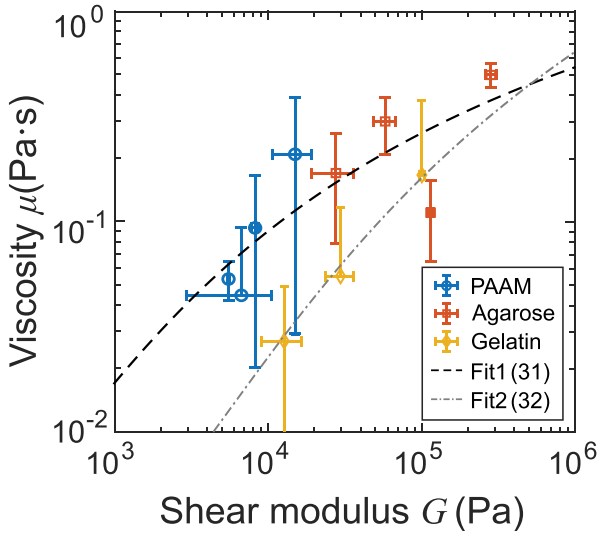

FIG. 4. Fitted material viscosity (μ) vs shear modulus G from laser-induced inertial cavitation (LIC) experimental measurements.[12,14,16] Fit1 and Fit2 are for static (i.e., PAAM and agarose) and dynamic (i.e., gelatin) crosslinks hydrogels, respectively.

IV. DISCUSSION AND CONCLUSION

Laser-induced cavitation (LIC) affords the user the flexibility of generating micrometer to centimeter-sized bubbles in a spatially controllable and repeatable fashion. Estimating the material properties using LIC such as with IMR requires the optical resolution of the resulting bubble kinematics, which limits its current application to nominally transparent materials. The emanation of two clearly distinguishable acoustic shocks, one at bubble initiation and one at first bubble collapse, allows recording of a well-defined bubble collapse time, which we have shown is strongly dependent on the stiffness of the surrounding material and can be cast in the form of a modified Rayleigh collapse time (24). The large amplitude of both of these pressure waves allows them to be easily recorded in the far field, which makes this approach, as described by Algorithm 1, attractive for estimating high strain rate material properties of optically opaque materials.

We find that the estimated viscoelastic properties of three commonly used hydrogels are similar whether using the knowledge of t_c and $R_{\max}$, or solely using the measurement of the bubble collapse time t_c. When comparing the results obtained via Algorithm 1 to the material properties obtained from IMR as a ground truth estimate, we find that the results are close except for 6% and 14% gelatin hydrogel cases. This is to be expected since the 6% and 14% gelatin concentration results also deviate from our theoretical predictions in Fig. 3. We also find that the relative errors of the estimated material properties are less for stiffer hydrogels. In general, when the shear modulus is $G > 10$ kPa, the relative errors of the shear modulus G and viscosity μ are less than 20% and 40%, respectively.

Finally, we conclude with a few limitations and observations. First, estimating a material's mechanical properties based on its characteristic Rayleigh collapse time is most accurate for larger (i.e., $R_{\max} > 80$ μm) bubbles in stiffer materials (shear modulus > 10 kPa). For smaller bubbles, the scaling behavior is more complex (Fig. 3) as predicted by Eq. (24) and will require additional treatment beyond the scope of this work. Furthermore, if the material is softer than 10 kPa, the modified Rayleigh collapse time approaches the collapse time in water and becomes nearly independent of the shear modulus of the materials, significantly limiting our model's ability to provide meaningful material information. Second, when $G/p_\infty \to 0$, $\psi \to 0.915$ in the Rayleigh–Plesset equation (15) and $\psi \to 0.933$ in the Keller–Miksis equation (17) (see supplementary material Fig. S5). Compared to the RP equation, the KM equation solved collapse time has been elongated about $(0.933–0.915)/0.915 \approx 1.97\%$, which implies the effects of compressibility on collapse time. Third, our current energy-based framework does not explicitly account for the effect of material viscosity and dissipation but rather offers an empirical solution via a correction factor and a phenomenological fit for its determination. Future studies can improve upon this by potentially accounting for this within the framework itself.[37,38] Finally, the choice of a hyperelastic neo-Hookean solid for the elastic contribution of the material model can be modified by the user to perhaps more appropriately represent the material. As can be seen from Fig. 3, that this particular choice in constitutive model agrees reasonably well with the three hydrogels examined here.

In summary, we derived and presented a new modified Rayleigh collapse time, t_c, for soft solids analogous to what has been derived for pure fluids. As t_c strongly depends on the shear modulus of the surrounding material, we showed that knowledge of t_c along with an estimate of R_{max}, the maximum bubble radius, during laser-induced inertial cavitation, can provide a meaningful estimate of the underlying high strain-rate material properties.

SUPPLEMENTARY MATERIAL

See the supplementary material for (i) a summary of all used laser induced inertial microcavitation (IMR) experimental data points, (ii) fitted empirical relation between maximum circumferential stretch ratio and the surrounding material's shear modulus, (iii) comparison of numerically simulated and experimentally measured bubble collapse times in bulk gel systems, (iv) fitted coefficient θ to include all other effects due to viscosity and bubble size, and (v) effects of compressibility on collapse time.

ACKNOWLEDGMENTS

We gratefully acknowledge support from the U.S. Office of Naval Research under PANTHER Award No. N000142112044 through Dr. Timothy Bentley.

AUTHOR DECLARATIONS

Conflict of Interest

The authors have no conflicts to disclose.

Author Contributions

Jin Yang: Conceptualization (equal); Data curation (equal); Formal analysis (equal); Investigation (equal); Methodology (equal); Software (equal); Visualization (equal); Writing – original draft (equal); Writing – review & editing (equal). **Alexander McGhee:** Data curation (equal); Resources (equal); Writing – review & editing (equal). **Griffin Radtke:** Data curation (equal); Writing – review & editing (equal). **Mauro Rodriguez:** Writing – review & editing (equal). **Christian Franck:** Funding acquisition (equal); Investigation (equal); Methodology (equal); Project administration (equal); Supervision (equal); Writing – review & editing (equal).

DATA AVAILABILITY

The data that support the findings of this study are available from the corresponding author upon reasonable request.

APPENDIX: DERIVATION OF EQ. (9)

After introducing stretch ratio parameter $\lambda := r/r_0$ and using Eq. (3), we can rewrite r and dr in terms of λ,

$$r = \left(R^3 - R_0^3\right)^{1/3} \lambda \left(\lambda^3 - 1\right)^{-1/3}, \tag{A1}$$

$$\mathrm{d}r = -\left(R^3 - R_0^3\right)^{1/3} \left(\lambda^3 - 1\right)^{-4/3} \mathrm{d}\lambda. \tag{A2}$$

Equation (7) can be further simplified as

$$\begin{aligned} E_{\text{Elastic}} &= \int_R^\infty 4\pi r^2 \frac{G}{2} \left[\left(\frac{r_0}{r}\right)^4 + 2\left(\frac{r}{r_0}\right)^2 - 3 \right] \mathrm{d}r, \\ &= 4\pi \left(R^3 - R_0^3\right) \int_1^{R/R_0} \frac{\lambda^2 W_{\text{NH}}(\lambda)}{\left(\lambda^3 - 1\right)^2} \mathrm{d}\lambda, \\ &= 2\pi G \left(R^3 - R_0^3\right) \left(\frac{2}{3} - \frac{R_0}{R} + \frac{R^2}{R^2 + RR_0 + R_0^2} \right). \end{aligned} \tag{A3}$$

REFERENCES

[1] C. E. Brennen, "Cavitation in medicine," Interface Focus **5**, 20150022 (2015).
[2] C. W. Barney, C. E. Dougan, K. R. McLeod, A. Kazemi-Moridani, Y. Zheng, Z. Ye, S. Tiwari, I. Sacligil, R. A. Riggleman, and S. Cai, "Cavitation in soft matter," Proc. Natl. Acad. Sci. U. S. A. **117**, 9157–9165 (2020).
[3] S. Tiwari, A. Kazemi-Moridani, Y. Zheng, C. W. Barney, K. R. McLeod, C. E. Dougan, A. J. Crosby, G. N. Tew, S. R. Peyton, S. Cai, and J.-H. Lee, "Seeded laser-induced cavitation for studying high-strain-rate irreversible deformation of soft materials," Soft Matter **16**, 9006–9013 (2020).
[4] E. Vlaisavljevich, Y. Kim, S. Allen, G. Owens, S. Pelletier, C. Cain, K. Ives, and Z. Xu, "Image-guided non-invasive ultrasound liver ablation using histotripsy: Feasibility study in an in vivo porcine model," Ultrasound Med. Biol. **39**, 1398–1409 (2013).
[5] K. B. Bader, E. Vlaisavljevich, and A. D. Maxwell, "For whom the bubble grows: Physical principles of bubble nucleation and dynamics in histotripsy ultrasound therapy," Ultrasound Med. Biol. **45**, 1056–1080 (2019).
[6] L. Mancia, M. Rodriguez, J. Sukovich, Z. Xu, and E. Johnsen, "Single–bubble dynamics in histotripsy and high–amplitude ultrasound: Modeling and validation," Phys. Med. Biol. **65**, 225014 (2020).
[7] L. Mancia, J. Yang, J.-S. Spratt, J. R. Sukovich, Z. Xu, T. Colonius, C. Franck, and E. Johnsen, "Acoustic cavitation rheometry," Soft Matter **17**, 2931–2941 (2021).
[8] R. W. Carlsen, A. L. Fawzi, Y. Wan, H. Kesari, and C. Franck, "A quantitative relationship between rotational head kinematics and brain tissue strain from a 2-D parametric finite element analysis," Brain Multiphys. **2**, 100024 (2021).
[9] R. Terpsma, R. W. Carlsen, R. Szalkowski, S. Malave, A. L. Fawzi, C. Franck, and C. Hovey, "Head impact modeling to support a rotational combat helmet drop test," Mil. Med. **188**, e745–e752 (2023).
[10] J. B. Estrada, C. Barajas, D. L. Henann, E. Johnsen, and C. Franck, "High strain-rate soft material characterization via inertial cavitation," J. Mech. Phys. Solids **112**, 291–317 (2018).
[11] J. Yang and C. Franck, "Strain stiffening effects of soft viscoelastic materials in inertial microcavitation," in *Dynamic Behavior of Materials*, edited by L. E. Lamberson (Springer International Publishing, Cham, 2020), Vol. 1, pp. 175–179.
[12] J. Yang, H. C. Cramer, and C. Franck, "Extracting non-linear viscoelastic material properties from violently-collapsing cavitation bubbles," Extreme Mech. Lett. **39**, 100839 (2020).
[13] J. Yang, H. C. Cramer, and C. Franck, "Dynamic Rugae strain localizations and instabilities in soft viscoelastic materials during inertial microcavitation," in *Dynamic Behavior of Materials*, edited by L. Lamberson, S. Mates, and V. Eliasson (Springer International Publishing, Cham, 2021), Vol. 1, pp. 45–49.
[14] J. Yang, H. C. Cramer, E. C. Bremer, S. Buyukozturk, Y. Yin, and C. Franck, "Mechanical characterization of agarose hydrogels and their inherent dynamic instabilities at ballistic to ultra-high strain-rates via inertial microcavitation," Extreme Mech. Lett. **51**, 101572 (2022).
[15] S. Buyukozturk, J.-S. Spratt, D. L. Henann, T. Colonius, and C. Franck, "Particle-assisted laser-induced inertial cavitation for high strain-rate soft material characterization," Exp. Mech. **62**, 1037–1050 (2022).
[16] A. McGhee, J. Yang, E. C. Bremer, Z. Xu, H. C. Cramer, J. B. Estrada, D. L. Henann, and C. Franck, "High-speed, full-field deformation measurements near inertial microcavitation bubbles inside viscoelastic hydrogels," Exp. Mech. **63**, 63–78 (2023).

[17]E.-A. Brujan, "Shock wave emission and cavitation bubble dynamics by femtosecond optical breakdown in polymer solutions," Ultrason. Sonochem. **58**, 104694 (2019).
[18]S. R. Gonzalez-Avila, F. Denner, and C.-D. Ohl, "The acoustic pressure generated by the cavitation bubble expansion and collapse near a rigid wall," Phys. Fluids **33**, 032118 (2021).
[19]F. Denner and S. Schenke, "Modeling acoustic emissions and shock formation of cavitation bubbles," Phys. Fluids **35**, 012114 (2023).
[20]F. Denner and S. Schenke, "APECSS: A software library for cavitation bubble dynamics and acoustic emissions," J. Open Source Software **8**, 5435 (2023).
[21]V.-T. Nguyen, T.-H. Phan, and W.-G. Park, "Modeling of shock wave produced by collapse of cavitation bubble using a fully conservative multiphase model," Phys. Fluids **35**, 116102 (2023).
[22]S. C. Haskell, N. Lu, G. E. Stocker, Z. Xu, and J. R. Sukovich, "Monitoring cavitation dynamics evolution in tissue mimicking hydrogels for repeated exposures via acoustic cavitation emissions," J. Acoust. Soc. Am. **153**, 237–247 (2023).
[23]L. Rayleigh, "VIII. On the pressure developed in a liquid during the collapse of a spherical cavity," London, Edinburgh, Dublin Philos. Mag. J. Sci. **34**, 94–98 (1917).
[24]W. Lauterborn, "High-speed photography of laser-induced breakdown in liquids," Appl. Phys. Lett. **21**, 27–29 (1972).
[25]A. A. Doinikov, "Translational motion of a spherical bubble in an acoustic standing wave of high intensity," Phys. Fluids **14**, 1420–1425 (2002).
[26]K. Johansen and M. Postema, "Lagrangian formalism for computing oscillations of spherically symmetric encapsulated acoustic antibubbles," Hydroacoustics **19**, 197–207 (2016).
[27]A. L. D. Barros, Á. L. Nogueira, R. C. Paschoal, D. Portes, and H. Rodrigues, "Dynamics of single-bubble sonoluminescence. An alternative approach to the Rayleigh–Plesset equation," Eur. J. Phys. **39**, 025807 (2018).
[28]C. Barajas and E. Johnsen, "The effects of heat and mass diffusion on freely oscillating bubbles in a viscoelastic, tissue-like medium," J. Acoust. Soc. Am. **141**, 908–918 (2017).
[29]A. Tzoumaka, J. Yang, S. Buyukozturk, C. Franck, and D. L. Henann, "Modeling high strain-rate microcavitation in soft materials: The role of material behavior in bubble dynamics," Soft Matter **19**, 3895–3909 (2023).
[30]M. Kim, "Energy transport during growth and collapse of a cavitation bubble," Ph.D. thesis (University of Michigan, Ann-Arbor, 2022).
[31]E. C. Bremer-Sai, J. Yang, A. McGhee, and C. Franck, "Ballistic and blast-relevant, high-rate material properties of physically and chemically crosslinked hydrogels" (submitted).
[32]Z. Hu, L. Xu, C.-Y. Chien, Y. Yang, Y. Gong, D. Ye, C. P. Pacia, and H. Chen, "3-D transcranial microbubble cavitation localization by four sensors," IEEE Trans. Ultrason, Ferroelectr., Freq. Control **68**, 3336–3346 (2021).
[33]G. T. Bokman, L. Biasiori-Poulanges, B. Lukić, C. Bourquard, D. W. Meyer, A. Rack, and O. Supponen, "High-speed X-ray phase-contrast imaging of single cavitation bubbles near a solid boundary," Phys. Fluids **35**, 013322 (2023).
[34]G. Latour, G. Georges, L. S. Lamoine, C. Deumié, J. Conrath, and L. Hoffart, "Human graft cornea and laser incisions imaging with micrometer scale resolution full-field optical coherence tomography," J. Biomed. Opt. **15**, 056006 (2010).
[35]N. Katta, A. B. McElroy, A. D. Estrada, and T. E. Milner, "Optical coherence tomography image-guided smart laser knife for surgery," Lasers Surg. Med. **50**, 202–212 (2018).
[36]B. Verhaagen and D. F. Rivas, "Measuring cavitation and its cleaning effect," Ultrason. Sonochem. **29**, 619–628 (2016).
[37]A. Zhang, S.-M. Li, P. Cui, S. Li, and Y.-L. Liu, "A unified theory for bubble dynamics," Phys. Fluids **35**, 033323 (2023).
[38]Z. Zhu, B. A. Abeid, and J. B. Estrada, "Reduced-order approach for soft material inertial cavitation rheometry," arXiv:2302.04227 (2023).